UROLOGIC ONCOLOGY

Seminar article

Clinical application of a 3D ultrasound-guided prostate biopsy system

Shyam Natarajan, M.S.[a,*], Leonard S. Marks, M.D.[b], Daniel J.A. Margolis, M.D.[c],
Jiaoti Huang, M.D., Ph.D.[d], Maria Luz Macairan, M.D.[b], Patricia Lieu[b],
Aaron Fenster, Ph.D.[e]

[a] Biomedical Engineering IDP, University of California, Los Angeles, CA 90095, USA
[b] Department of Urology, David Geffen School of Medicine, University of California, Los Angeles, CA 90095, USA
[c] Department of Radiology, David Geffen School of Medicine, University of California, Los Angeles, CA 90095, USA
[d] Department of Pathology, David Geffen School of Medicine, University of California, Los Angeles, CA 90095, USA
[e] Robarts Research Institute, University of Western Ontario, London, Ontario, Canada

Abstract

Objectives: Prostate biopsy (Bx) has for 3 decades been performed in a systematic, but blind fashion using 2D ultrasound (US). Herein is described the initial clinical evaluation of a 3D Bx tracking and targeting device (Artemis; Eigen, Grass Valley, CA). Our main objective was to test accuracy of the new 3D method in men undergoing first and follow-up Bx to rule out prostate cancer (CaP).

Materials and methods: Patients in the study were men ages 35–87 years (66.1 ± 9.9), scheduled for Bx to rule out CaP, who entered into an IRB-approved protocol. A total of 218 subjects underwent conventional trans-rectal US (TRUS); the tracking system was then attached to the US probe; the prostate was scanned and a 3D reconstruction was created. All Bx sites were visualized in 3D and tracked electronically. In 11 men, a pilot study was conducted to test ability of the device to return a Bx to an original site. In 47 men, multi-parametric 3 Tesla MRI, incorporating T2-weighted images, dynamic contrast enhancement, and diffusion-weighted imaging, was performed in advance of the TRUS, allowing the stored MRI images to be fused with real-time US during biopsy. Lesions on MRI were delineated by a radiologist, assigned a grade of CaP suspicion, and fused into TRUS for biopsy targeting.

Results: 3D Bx tracking was completed successfully in 180/218 patients, with a success rate approaching 95% among the last 50 men. Average time for Bx with the Artemis device was 15 minutes with an additional 5 minutes for MRI fusion and Bx targeting. In the tracking study, an ability to return to prior Bx sites ($n = 32$) within 1.2 ± 1.1 mm SD was demonstrated and was independent of prostate volume or location of Bx site. In the MRI fusion study, when suspicious lesions were targeted, a 33% Bx-positivity rate was found compared with a 7% positivity rate for systematic, nontargeted Bx (19/57 cores vs. 9/124 cores, $P = 0.03$).

Conclusion: Use of 3D tracking and image fusion has the potential to transform MRI into a clinical tool to aid biopsy and improve current methods for diagnosis and follow-up of CaP. © 2011 Elsevier Inc. All rights reserved.

Keywords: Prostate; Cancer; Artemis; Biopsy; MRI; Diffusion weighted imaging

1. Introduction

"The discovery that would have the greatest impact on our field would be the development of accurate imaging of tumor within the prostate." —Patrick C. Walsh [1].

Imaging prostate cancer (CaP), while in a curable state, has proven elusive, despite a half-century of interest and effort. Virtually all major cancers can be easily imaged within the organ of origin, but not CaP. Thus, diagnosis of CaP is often fortuitous, materializing only when systematic biopsy, which is usually driven by an elevated PSA level, is positive [2]. However, recent developments in magnetic resonance imaging (MRI) technologies—3 Tesla magnets and a multi-parametric approach—have led to a promising advance in prostate cancer imaging. Moreover, fusion of ultrasound and MRI by a new technology appears capable of bringing those images to the patient for biopsy guidance. Challenges to imaging cancer within the prostate include (1) histologic similarity of cancer and benign tissue in many cases, (2) heterogeneity of prostate tissue in aging men, (3)

* Corresponding author. Tel.: +1-310-206-5545; fax: +1-310-206-5545.
E-mail address: shyam@ucla.edu (S. Natarajan).

decreasing volumes of CaP found today as a result of early biopsy stimulated by PSA levels, and (4) limited resolving power of available imaging devices. Systematic biopsy often detects insignificant cancers [3], which cannot reliably be distinguished by available biomarkers [4], and treatment decisions based on biopsy alone may be problematic. Overtreatment of localized CaP has been increasingly recognized [5], and active surveillance is gaining traction as a first choice for many men judged to have 'low-risk' CaP [6,7]. In two groups especially—men undergoing active surveillance and those with elevated PSA levels but negative biopsies—the ability to image CaP within the prostate (or exclude it) could help clarify characteristics of the underlying pathology.

Recent advances in magnetic resonance imaging may soon alter the landscape of CaP diagnosis. As detailed below, MRI has evolved to yield images within the prostate that are approaching a considerable degree of diagnostic accuracy [8–11]. The increased accuracy is attributable to machines that employ powerful 3 Tesla magnets, diffusion weighted imaging, and dynamic contrast enhancement. However, direct prostate biopsy within MRI machines is largely restricted to research institutions [8]. We tested a new device (Artemis; Eigen, Grass Valley, CA), which allows biopsy site tracking in ultrasound and fusion of real-time ultrasound with MRI. FDA approval [510(k)] was granted to the manufacturer in May 2008, but testing to date has been entirely on phantoms. We became early adopters of this technology, hoping to increase accuracy of prostate tissue sampling by recording biopsy sites and incorporating multi-parametric MRI detail into the site selection process. Development of the new technology at UCLA has involved an integrated collaboration between urology, radiology, pathology, and biomedical engineering. The program goals are to improve accuracy of prostate biopsy, to develop a method for visual follow-up and tissue sampling of 'low risk' lesions and, potentially, to aid in focal therapy. Herein we present an initial experience with the device, based on studies in the first 218 men who underwent 3D systematic biopsy in 2009–2010, 47 of whom underwent MRI/TRUS fusion biopsy.

2. Magnetic resonance imaging of prostate cancer

Magnetic resonance imaging has been used to evaluate the prostate and surrounding structures for nearly a quarter century [12]. Initially, investigators utilized the increased signal-to-noise ratio from the use of endorectal coils to study T1- and T2-weighted imaging (T2WI) and spectroscopic imaging for local staging [13–16]. Standard T2-weighted imaging provides excellent resolution, but does not discriminate cancer from other processes with acceptable accuracy [17,18].

Diffusion-weighted imaging (DWI) and dynamic contrast imaging (DCE), products of the past decade, appear likely to increase accuracy of prostate cancer detection.

When added to T2-weighted imaging, these techniques constitute a form of "multi-parametric" MRI. The use of multiple MR sequences in the detection of localized CaP has shown to improve sensitivity over any single parameter [19–23]. Furthermore, the use of multiparametric imaging may also enhance overall accuracy in cancer diagnosis [24,25]. The use of multiple parameters also appears to improve biopsy yield, both MR- and US-guided [11,26–29]. Spectroscopy has also been evaluated in this context, but has not been shown to improve diagnostic accuracy when added to other imaging parameters [30–33]. Spectroscopy via endorectal coil is used for preoperative staging, but appears to add little in the diagnosis of intracapsular lesions [8,34,35].

Dynamic contrast enhanced (DCE) MRI allows for the visualization of blood perfusion, via a bolus injection of gadolinium contrast during rapidly repeated scanning with high temporal resolution. The use of DCE MRI for the detection of prostate cancer has been validated for over a decade [15,16]. DCE, modeled using pharmacokinetic parameters, is thought to be able to accurately image vascular pathophysiology, such as angiogenesis [20,36]. Furthermore, prior studies have suggested a correlation of such parameters with the histologic grade of disease [37,38]. Both simple and complex models of DCE have been shown useful for the detection of prostate cancer [17,21,24,39,40].

Diffusion weighted imaging (DWI) involves the quantification of free water motion, also known as "Brownian" motion, such that a lower apparent diffusion coefficient (ADC) corresponds to greater restriction in free water motion. Prostate cancer tissues restrict free water motion, likely on the basis of increased cellularity compared with normal prostate tissue [41–43]. The addition of diffusion-weighted imaging (DWI) to prostate MRI improves sensitivity and specificity for both peripheral and central gland disease [44–49] and has been shown useful for localization of biopsy targets in high risk patients who are initially biopsy-negative [26]. The degree of diffusion restriction also appears to correlate with Gleason score, perhaps reflecting cellular density [48,50]. Low ADC values are reported to correlate with unfavorable histology on repeat biopsy in men on active surveillance [51].

3. MR technique and interpretation

In our current work, we utilize multiparametric MRI (T2WI, DWI, and DCE) to prospectively assess likelihood of prostate cancer, and to improve CaP detection through biopsy. A transabdominal coil is used (1) to minimize patient discomfort and (2) because with multiparametric techniques, the endorectal approach does not appear necessary for detection and grade stratification [8,52]. Imaging is performed on a Siemens TrioTim Somatom 3T (Siemens Medical Solutions, Malvern, PA) magnet with high-performance gradients using a multi-channel external phased-

Table 1
MR imaging parameters

Pulse sequence	TR/TE (ms)	Slice/gap	Matrix/FOV cm	Parameters
T2:3D TSE	3800–5040/101	1.5/0 mm	256 × 205/14 × 14	ETL 13
DWI:EPI	1600–2300/75–90	5/1.65 mm	256 × 154/35 × 26	b = 400/800/1000
DCE: TWIST	2.7/1.1 (10° FA)	1.5/0 mm	320 × 225/28 × 30	See below

*Dynamic contrast enhancement protocol involved 42 acquisitions every 6.1 seconds, with 0.1 mg/kg gadopentetate dimeglumine (Magnevist, Bayer) administered at 2 mL/s after the second acquisition for baseline calculation.

array coil. The protocol used in this investigation is provided in Table 1.

Each of the 3 MRI parameters utilized are interpreted by a radiologist (D.M.), and suspicious areas, or regions of interest (ROI), are identified on a DICOM viewer (CADstream; Merge Healthcare, Chicago, IL). MR interpretation is blinded with respect to the patient history and prior imaging (Fig. 1).

ROIs seen on each MR parameter are assigned image grades on a 1–5 scale, with "1" being unsuspicious and "5" as very suspicious of CaP. The overall level of suspicion is a composite score determined primarily by the apparent diffusion coefficient (ADC) and secondarily by the T2 and DCE appearance. The degree of suspicion for T2 is based on the degree of signal darkening as well as the presence of mass effect or surrounding distortion. ADC suspicion is graded based on numerical values —1.2 mm^2/s and above is 1, 1.0–1.2 mm^2/s is 2, 0.8–1.0 mm^2/s is 3, 0.6–0.8 mm^2/s is 4, and below 0.6 mm^2/s is 5. These numbers are lower than those reported in the literature, because only high b values were used to reduce the perfusion component of the ADC. The perfusion grading system is based on 3 components:
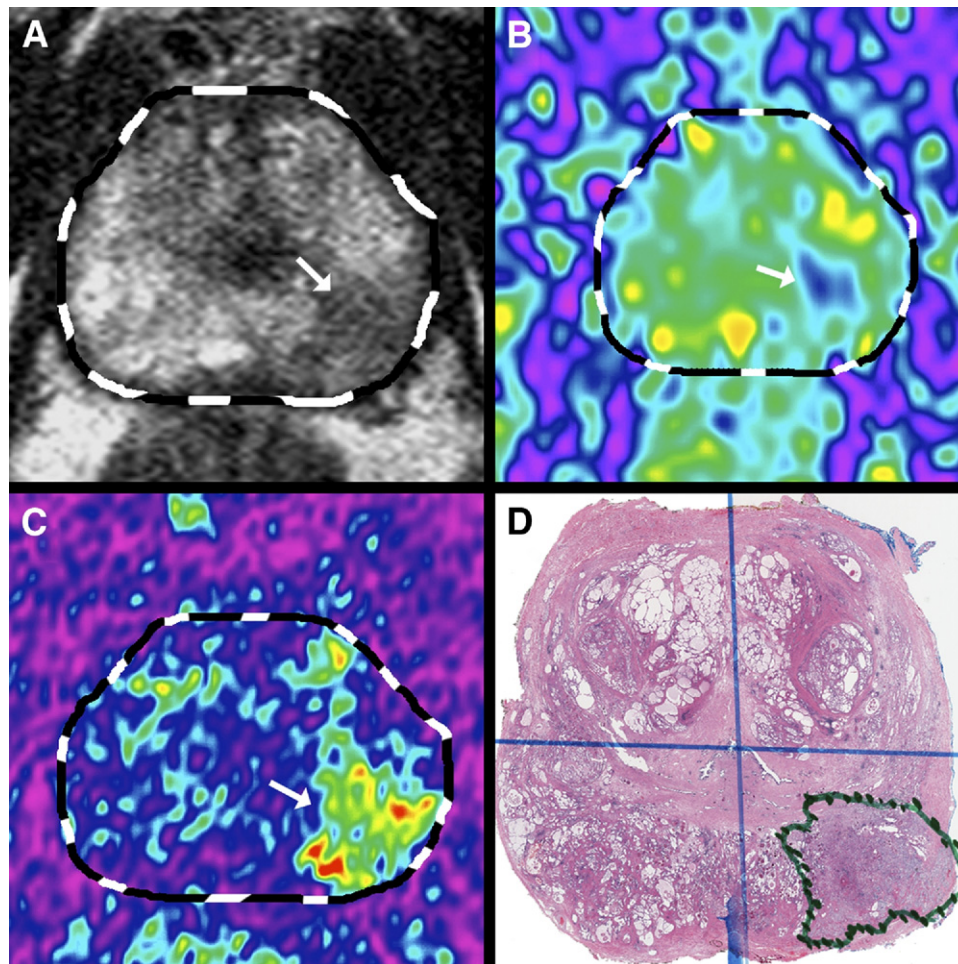

Fig. 1. Localized prostate cancer, visualized by MRI (image grade 5) on (A) T2-weighted image, (B) diffusion weighted image, and (C) dynamic contrast enhancement. (D) Whole-mount study of radical prostatectomy specimen confirmed MRI findings. Tumor was adenocarcinoma, Gleason score 3+3 = 6, and was correctly identified by targeted biopsy employing MRI fusion with real-time ultrasound. (Color version of figure is available online.)

Table 2
Image grading system for regions of interest found on multi-parametric MRI

Image grade	T2-weighted imaging (T2WI)	Apparent diffusion coefficient (ADC)	Dynamic contrast enhancement (DCE)
1	Normal	$>1.2 \times 10^{-3}$ mm^2/s	Normal
2	Faint decreased signal	$1.0–1.2 \times 10^{-3}$ mm^2/s	Mildly abnormal enhancement
3	Moderately dark nodule	$0.8–1.0 \times 10^{-3}$ mm^2/s	Moderately abnormal enhancement
4	Intensely dark nodule	$0.6–0.8 \times 10^{-3}$ mm^2/s	Highly abnormal enhancement
5	Dark nodule with mass effect	$<0.6 \times 10^{-3}$ mm^2/s	Profoundly abnormal enhancement

rapid wash-in (or early enhancement), intensity of enhancement, and washout. When rapid wash-in is intense, this also increases the perfusion grade. DCE suspicion is given a point for rapid wash-in, intense enhancement, and washout, with 1 more point for intense early enhancement (Table 2).

4. Clinical evaluation of targeted biopsy

The Artemis device is a 3D ultrasound-guided prostate biopsy system [53] that provides tracking of biopsy sites within the prostate [54]. The device software also allows stored MRI images to be electronically transferred and fused with real-time ultrasound, allowing biopsy needles to be guided into targets. The current version of this device evolved from a prototype built at the Robarts Research Institute in London, Ontario, Canada (Fig. 2) [53]. At Robarts Research, an affiliate of the University of Western Ontario, a team of several hundred scientists has been assembled under the direction of Aaron Fenster, Ph.D., to advance medical imaging. Interest in 3D ultrasonic imaging, which is the core utility of the Artemis device, dates from pioneering efforts at Robarts over the past 2 decades [55].

An Artemis unit was installed in the Clark Urological Center at UCLA in March 2009, and clinical work with the device began shortly thereafter. Approval from the UCLA Institutional Review Board was obtained. Our current experience includes 218 patients with systematic

biopsy under 3D guidance, 47 of whom had an MRI prior to biopsy and underwent targeted biopsy with MR fusion. Patients in the study were men with an average age of 66.1 ± 9.9 years (range, 35–87). For men suspected of CaP, initial biopsy sets are tracked with the device; pre-biopsy MRI and MRI/TRUS fusion was reserved for men in active surveillance or in men with prior negative biopsies and persistently elevated PSA levels. We concur with the rationale for selective use of pre-biopsy MRI, recently espoused by others [56,57]. Systematic biopsy under 3D guidance was completed successfully in 180/218 patients, with a success rate approaching 95% among the last 50 men. Reasons for failure of 3D guidance included difficulties in positioning the tracking arm, software issues early on, and poor patient compliance. In these instances, procedures were converted to freehand biopsy.

5. Delineation of suspicious areas

Suspicious areas, or regions of interest (ROI), were located on each MR parameter during interpretation, and a suspicion index (image grade) was assigned to each (Table 2). The ROI was then delineated in multiple 1–3 mm slices on the axial T2-weighted images using a contour tool in a DICOM reader (OsiriX [58]). A smooth 3D model of the ROI was then formed, and spatial coordinates of the model were output to a text file. This process was repeated for each
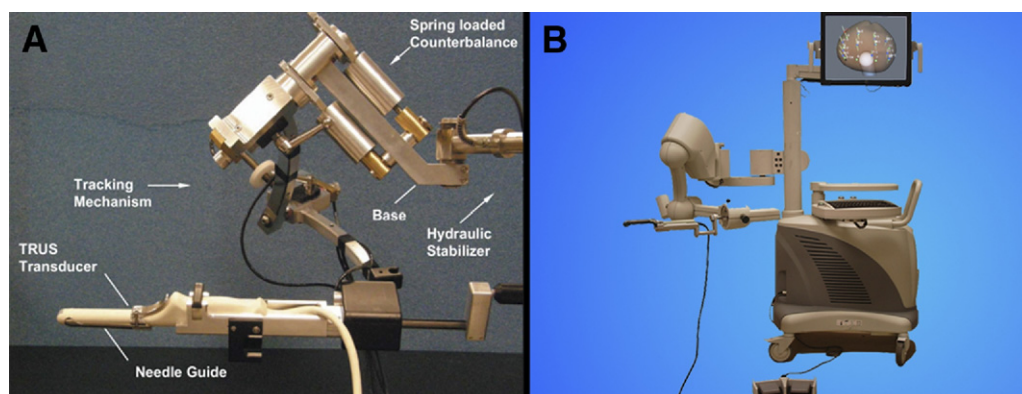

Fig. 2. 3D biopsy tracking system. (A) Prototype built at Robarts Research Institute, London, Ontario, Canada, and (B) current version (Artemis) developed by Eigen. The main components are a tracking arm, monitor, and digital video processor. (Color version of figure is available online.)
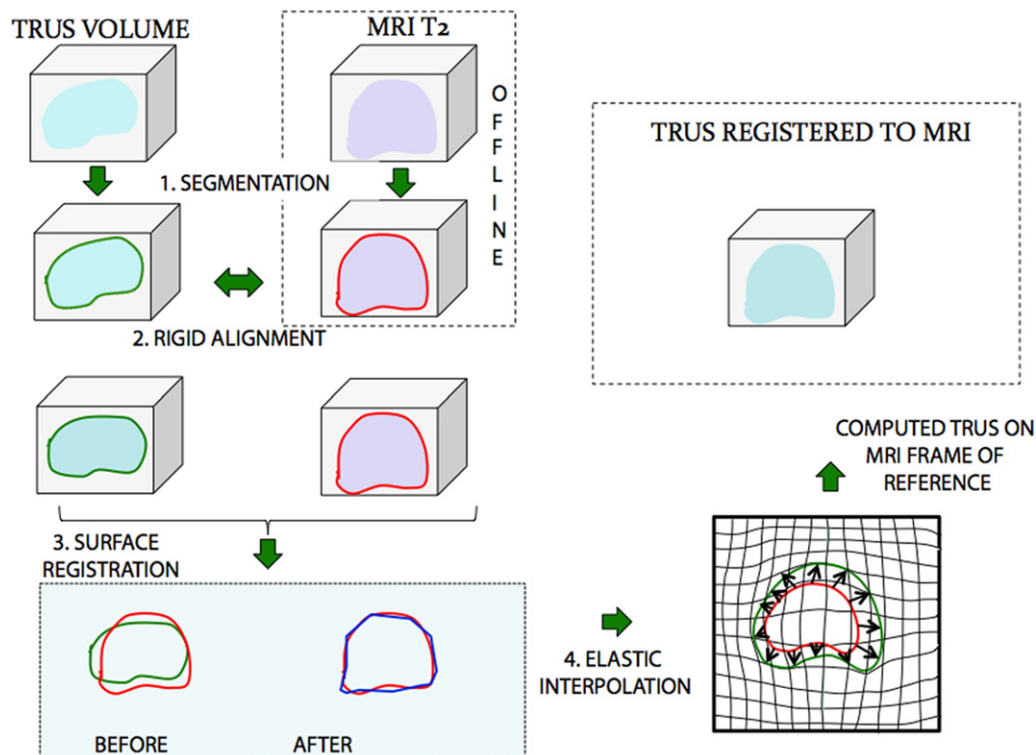
Fig. 3. Process of MR Fusion. MR and TRUS images were segmented (1) and then rigidly aligned (2). Fusion then proceeded, involving a surface registration (3), and elastic (non-rigid) interpolation (4). (Color version of figure is available online.)

suspicious area, resulting in a 3D model for each ROI. These files were then imported into 3D ultrasound system via CD and were used for biopsy targeting. The axial T2-weighted MR DICOM images were also imported with the same CD in order to visualize the MR and TRUS images side-by-side.

6. Biopsy technique

Biopsy was performed using a conventional spring-loaded gun and 18 ga needles. A preliminary cleansing enema and prophylactic quinolone antibiotic were used. Procedures began with the patient in left lateral decubitus position, using a conventional ultrasound probe and machine (Hitachi Hi-Vision 5500 [Hitachi Medical Systems America, Twinsburg, OH], 7.5 MHz end-fire) to image the prostate transrectally in transverse and longitudinal views. After a preliminary scan, the prostate was anesthetized with a peri-prostatic block, and a geometric volume determination (L*W*H/2) was obtained. Next, the tracking arm of the 3D biopsy system was attached to the ultrasound probe, keeping the arm in a horizontal orientation. The prostate was scanned, as the probe was rotated 200° across the surface of the organ. Ultrasonic images of the prostate were captured by the Artemis device and assembled into a 3D volume onscreen. Segmentation of the prostate (delineation of the prostate on TRUS) was performed, correcting the

scan as may be required for accurate margin identification [59,60]. The isolated prostate was then digitally reconstructed on the screen in real-time. Planimetric volumetry was performed automatically by the device, and similarity of the geometric and planimetric volume was confirmed (±20%).

A systematic array of 12 preselected biopsy sites was then loaded and displayed on the digital prostate model. Fusion commenced once the CD containing the MR and ROI information was inserted into the device. Prostate segmentation in MRI was performed prior to biopsy. During targeted biopsy with image fusion, the MRI was incorporated into the TRUS image by registering the two. Registration began by manual selection of fixed anatomical landmarks, such as the base and apex of the prostatic urethra, in both image modalities (Fig. 3). Once the 2 images were aligned, the delineated prostates on ultrasound were mapped to the MRI outline using a surface-based registration algorithm [61,62]. The 2 images were then considered registered, and an identical transformation was applied to the ROI models, which were subsequently displayed on the digital prostate model. Patient immobility after segmentation was critical for accurate registration. Biopsy cores were then obtained by aiming at the suspicious areas and/or the preselected sites displayed on the digital model (Fig. 4). Elapsed times were electronically recorded for all patients, and reflect time from beginning of TRUS scan to end of biopsy. Average time for systematic biopsy was estimated
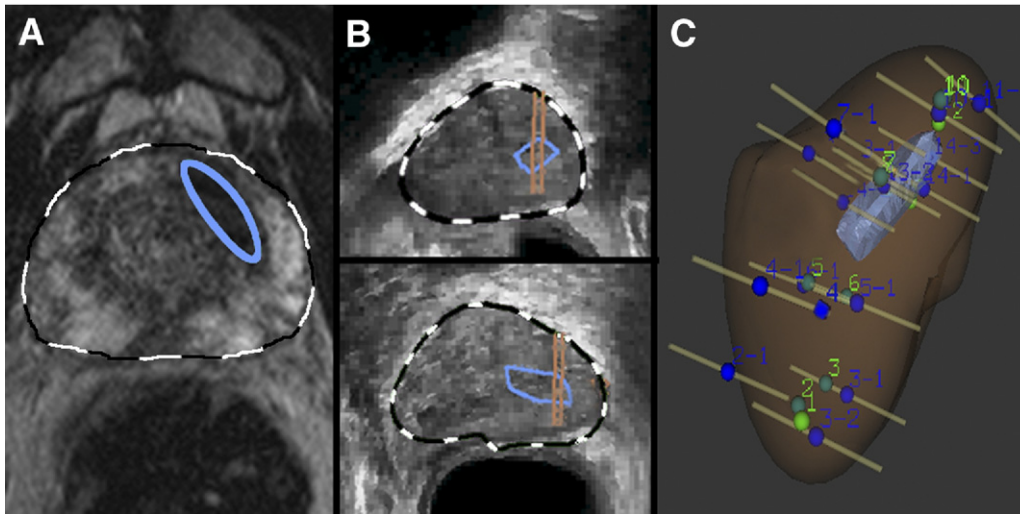
Fig. 4. Targeted biopsy using MR Fusion. (A) A lesion was identified on MRI (image grade 4) and delineated on T2WI by radiologist (blue ellipse). The axial T2WI and area of interest was fused with real-time ultrasound images. (B) Lesion was identified in sagittal and axial planes (blue enclosures), and biopsy-targeting of the lesion was established (parallel lines overlying blue enclosures). Both targeted and systematic biopsies were performed under real-time ultrasound guidance. (C) Sites of systematic and targeted biopsies were recorded within 3D reconstruction of prostate, confirming that several targeted biopsies penetrated region of interest. Biopsy results showed a Gleason score 3+3 = 6 cancer in only the targeted area. (Color version of figure is available online.)

to be 15 minutes, with an additional 5 minutes for MRI fusion and biopsy targeting.

7. Biopsy tracking accuracy

Clinical accuracy of 3D biopsy tracking was tested in 11 consecutive men, undergoing TRUS/Bx to rule out prostate cancer [54]. Locations of each biopsy site were recorded by the device and displayed on the digital model, as described above. The ultrasound probe was then removed, detached, and cleaned, while patients remained on the procedure table. The probe was then reinserted, and a new 3D scan of the prostate was performed, and prior biopsy sites were recalled. The subsequent scan was used for guidance, and prior biopsy sites as targets. Three randomly selected sites in each patient were re-biopsied. The distance between original and re-biopsy sites was determined in a blinded fashion using geometric analysis at Robarts Research. Results were stratified by prostate volume and site location (Table 3) [54]. Mean error (mm, target to center of re-biopsy core) for all 32 Bx was 1.2 ± 1.1 (range, 0.2–5.1)

and was independent of prostate volume or biopsy location. Reliability of the Artemis device to re-biopsy specific sites in the prostate was supported by results of this pilot, extending prior studies on phantoms (Fig. 5) [53].
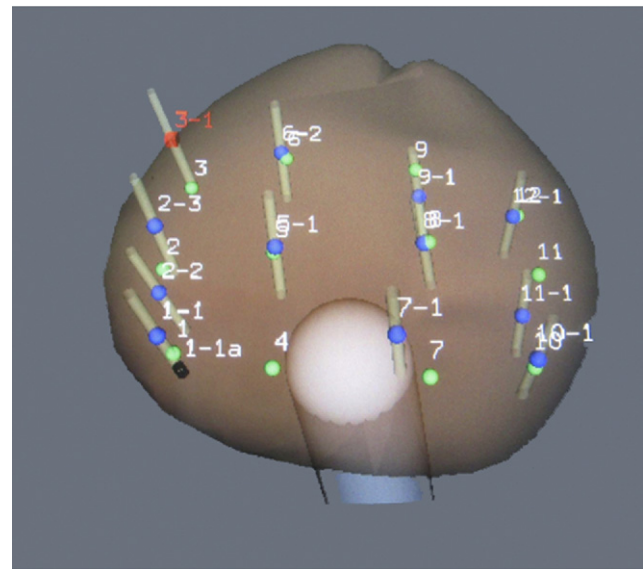
● = Target (center of initial Bx)
● = Repeat (center of repeat Bx)

Fig. 5. 3D reconstruction of prostate showing proximity of repeat biopsy sites (blue dots) to initial biopsy sites used as targets (green dots). In a pilot study, the average distance from repeat biopsy to target was 1.2 ± 1.1 mm and was independent of both volume and location within the prostate (Table 3). (Color version of figure is available online.)

Table 3
Clinical accuracy of repeat biopsy targeting (tracking)

Prostate volume (cc)	Patients (n)	Repeat biopsies (n)	Biopsy Error, mm (mean ± SD)	Carcinoma
<40	3	10	1.6 ± 1.5	0
41–60	5	12	1.0 ± 0.8	2
>60	3	10	1.1 ± 0.7	1
Total	11	32	1.2 ± 1.1	3

Table 4
Image grade of targets and probability of cancer

Image grade	Targets (n)	Patients (n)	Cancer (%)
1–2	16	13	0
3	33	29	24
4	14	12	57
5	2	2	50
Total	65	56*	23

* Patients with more than 1 target were counted in the table multiple times; 1 to 3 biopsy cores are taken of the ROI, depending on size of lesion.

8. Targeted biopsy with MR fusion

Accuracy of biopsy targeting was tested by comparing histologic results of targeted vs. systematic biopsy. Biopsy data were obtained on 47 men, in which 65 suspicious areas, or targets, were identified and biopsied. These men also underwent 12-core systematic biopsy. Of these men, 30 were found to have CaP. The high rate of positivity was likely due to the inclusion of men on active surveillance (18 men). Targeted biopsies were found to be more likely to reveal cancer than non-targeted biopsies and high-grade areas were more likely to be cancer than low-grade areas (Table 4). When high-grade ROIs were targeted, a 33% biopsy-positivity rate was found vs. a 7% positivity rate for systematic, nontargeted biopsies (19/57 cores vs. 9/124 cores, $P = 0.03$).

Of the 30 men found to have CaP, 9 were diagnosed using systematic biopsy only, 5 with MR fusion-guided biopsy only, and 16 with both protocols. Of the patients for whom only systematic cores were positive, 5 patients (55%) had cancer in the same sextant as the target, indicating mistargeting of the lesion. After a proper targeting technique was established, 12 of the last 22 patients with targets were positive for CaP upon biopsy. Three patients were diagnosed with CaP using systematic biopsy alone, 4 with targeted biopsy alone, and 5 using both protocols.

An additional benefit of 3D biopsy tracking may be an improved systematic biopsy, i.e., more evenly distributed sites than with conventional methods. We have observed through 3D tracking that unguided biopsy locations are not always symmetrically distributed and tend to be clustered, despite attempts at symmetric placement. Thus, in the above comparison, results with systematic biopsies may be favored by wider sampling from the built-in sites.

9. Comment

Technologies to improve accuracy of prostate biopsy are rapidly emerging. In selecting and following men for active surveillance, the new technologies are particularly compelling. In the future, men considering focal therapy may also benefit from improved biopsy accuracy. We have described an initial clinical experience with a new 3D ultrasound device, which allows biopsy-site tracking for future recall and fusion of MRI targets with real-time ultrasound. While promising, these early experiences have not yet conclusively shown the benefit of tracking and targeted biopsy with MR fusion. Challenges exist in terms of perfecting registration of ultrasound and MR images. The actual anatomic locations of tumor tissue are the final determinant of biopsy (and MR) accuracy. In this regard, whole-mount prostatectomy studies from men who have undergone both 3D targeted and systematic biopsy will be critical. Further refinements of the fusion technology are necessary before widespread clinical adoption is possible. These will likely include multiple areas of hardware miniaturization, which could improve ease of operation. Biopsy tracking and targeting with image fusion may become important tools to improve diagnosis and management of men with prostate cancer.

Acknowledgments

References

[1] Walsh PC. 2008 Whitmore Lecture: Radical prostatectomy–where we were and where we are going. Urol Oncol 2009;27:246–50.

[2] Stamey TA, Caldwell M, McNeal JE, et al. The prostate specific antigen era in the United States is over for prostate cancer: What happened in the last 20 years? J Urol 2004;172:1297–301.

[3] Epstein JI, Walsh PC, Carmichael M, et al. Pathologic and clinical findings to predict tumor extent of nonpalpable (stage T1c) prostate cancer. JAMA 1994;271:368–74.

[4] Sutcliffe P, Hummel S, Simpson E, et al. Use of classical and novel biomarkers as prognostic risk factors for localized prostate cancer: A systematic review. Health Technol Assess 2009;13:1–219.

[5] Cooperberg MR, Broering JM, Kantoff PW, et al. Contemporary trends in low risk prostate cancer: Risk assessment and treatment. J Urol 2007;178:S14–9.

[6] Carter HB, Sauvageot J, Walsh PC, et al. Prospective evaluation of men with stage T1c adenocarcinoma of the prostate. J Urol 1997; 157:2206–9.

[7] Klotz L, Zhang L, Lam A, et al. Clinical results of long-term follow-up of a large, active surveillance cohort with localized prostate cancer. J Clin Oncol 2010;28:126–31.

[8] Hambrock T, Somford DM, Hoeks C, et al. Magnetic resonance imaging guided prostate biopsy in men with repeat negative biopsies and increased prostate specific antigen. J Urol 2010;183:520–8.

[9] Hricak H, Choyke PL, Eberhardt SC, et al. Imaging prostate cancer: A multidisciplinary perspective. Radiology 2007;243:28–53.

[10] Kim CK, Park BK, Kim B. Diffusion-weighted MRI at 3 T for the evaluation of prostate cancer. Am J Roentgenol 2010;194:1461–9.

[11] Lawrentschuk N, Fleshner N. The role of magnetic resonance imaging in targeting prostate cancer in patients with previous negative

biopsies and elevated prostate-specific antigen levels. BJU international 2009;103:730–3.

[12] Dooms GC, Hricak H. Magnetic resonance imaging of the pelvis: Prostate and urinary bladder. Urol Radiol 1986;8:156–65.

[13] Narayan P, Vigneron DB, Jajodia P, et al. Transrectal probe for 1H MRI and 31P MR spectroscopy of the prostate gland. Magn Reson Med 1989;11:209–20.

[14] Outwater EK, Petersen RO, Siegelman ES, et al. Prostate carcinoma: Assessment of diagnostic criteria for capsular penetration on endorectal coil MR images. Radiology 1994;193:333–9.

[15] Brown G, Macvicar D, Ayton V, et al. The role of intravenous contrast enhancement in magnetic resonance imaging of prostatic carcinoma. Clin Radiol 1995;50:601–6.

[16] Jager G, Ruijter E, Van de Kaa C, et al. Dynamic TurboFLASH subtraction technique for contrast-enhanced MR imaging of the prostate: Correlation with histopathologic results. Radiology 1997;203:645–52.

[17] Engelbrecht MR, Huisman HJ, Laheij RJF, et al. Discrimination of prostate cancer from normal peripheral zone and central gland tissue by using dynamic contrast-enhanced MR imaging. Radiology 2003;229: 248.

[18] Quint L, Van Erp J, Bland P, et al. Prostate cancer: Correlation of MR images with tissue optical density at pathologic examination. Radiology 1991;179:837–42.

[19] Kozlowski P, Chang SD, Jones EC, et al. Combined diffusion-weighted and dynamic contrast-enhanced MRI for prostate cancer diagnosis—correlation with biopsy and histopathology. J Magn Reson 2006;24:108–13.

[20] Ocak I, Bernardo M, Metzger G, et al. Dynamic contrast-enhanced MRI of prostate cancer at 3 T: A study of pharmacokinetic parameters. Am J Roentgenol 2007;189:W192–201.

[21] Tanimoto A, Nakashima J, Kohno H, et al. Prostate cancer screening: The clinical value of diffusion-weighted imaging and dynamic MR imaging in combination with T2-weighted imaging. J Magn Reson 2007;25:146–52.

[22] Oto A, Kayhan A, Jiang Y, et al. Prostate cancer: Differentiation of central gland cancer from benign prostatic hyperplasia by using diffusion-weighted and dynamic contrast-enhanced MR imaging. Radiology 2010;257:715–23.

[23] Turkbey B, Xu S, Kruecker J, et al. Documenting the location of prostate biopsies with image fusion. BJU Intl 2010;107:53–7.

[24] Kitajima K, Kaji Y, Fukabori Y, et al. Prostate cancer detection with 3 T MRI: Comparison of diffusion-weighted imaging and dynamic contrast-enhanced MRI in combination with T2-weighted imaging. J Magn Reson 2010;31:625–31.

[25] Langer DL, van der Kwast TH, Evans AJ, et al. Prostate tissue composition and MR measurements: Investigating the relationships between ADC, T2, Ktrans, ve, and corresponding histologic features. Radiology 2010;255:485–94.

[26] Park BK, Lee HM, Kim CK, et al. Lesion localization in patients with a previous negative transrectal ultrasound biopsy and persistently elevated prostate specific antigen level using diffusion-weighted imaging at 3 Tesla before re-biopsy. Invest Radiol 2008;43:789–93.

[27] Xu S, Kruecker J, Turkbey B, et al. Real-time MRI-TRUS fusion for guidance of targeted prostate biopsies. Comp Aid Surg 2008;13:255–64.

[28] Turkbey B, Pinto PA, Mani H, et al. Prostate Cancer: Value of multiparametric MR imaging at 3 T for detection—histopathologic correlation. Radiology 2010;255:89–99.

[29] Rastinehad AR, Baccala AA, Chung PH, et al. D'Amico risk stratification correlates with degree of suspicion of prostate cancer on multiparametric magnetic resonance imaging. J Urol 2011;185:815–20.

[30] Fütterer JJ, Heijmink SW, Scheenen TWJ, et al. Prostate cancer localization with dynamic contrast-enhanced MR imaging and proton MR spectroscopic imaging. Radiology 2006;241:449–58.

[31] Chen M, Dang HD, Wang JY, et al. Prostate cancer detection: Comparison of T2-weighted imaging, diffusion-weighted imaging, proton magnetic resonance spectroscopic imaging, and the 3 techniques combined. Acta Radiologica 2008;49:602–10.

[32] Riches SF, Payne GS, Morgan VA, et al. MRI in the detection of prostate cancer: Combined apparent diffusion coefficient, metabolite ratio, and vascular parameters. Am J Roentgenol 2009;193:1583–91.

[33] Weinreb JC, Blume JD, Coakley FV, et al. Prostate cancer: Sextant localization at MR imaging and MR spectroscopic imaging before prostatectomy—results of ACRIN prospective multi-institutional clinicopathologic study. Radiology 2009;251:122–33.

[34] Heijmink SW, Fütterer JJ, Hambrock T, et al. Prostate cancer: Body-array vs. endorectal coil MR imaging at 3 T—comparison of image quality, localization, and staging performance. Radiology 2007;244:184–95.

[35] Park BK, Kim B, Kim CK, et al. Comparison of phased-array 3.0-T and endorectal 1.5-T magnetic resonance imaging in the evaluation of local staging accuracy for prostate cancer. J Comput Assist Tomogr 2007;31:534–8.

[36] Alonzi R, Padhani AR, Allen C. Dynamic contrast enhanced MRI in prostate cancer. Eur J Radiol 2007;63:335–50.

[37] van Dorsten FA, van der Graaf M, Engelbrecht MRW, et al. Combined quantitative dynamic contrast-enhanced MR imaging and 1H MR spectroscopic imaging of human prostate cancer. J Magn Reson Imaging 2004;20:279–87.

[38] Padhani AR, Gapinski CJ, Macvicar DA, et al. Dynamic contrast enhanced MRI of prostate cancer: Correlation with morphology and tumor stage, histological grade, and PSA. Clinical Radiol 2000;55:99–109.

[39] Fütterer JJ, Engelbrecht MR, Huisman HJ, et al. Staging prostate cancer with dynamic contrast-enhanced endorectal MR imaging prior to radical prostatectomy: Experienced vs. less experienced readers. Radiology 2005;237:541–9.

[40] Girouin N, Mege-Lechevallier F, Tonina Senes A, et al. Prostate dynamic contrast-enhanced MRI with simple visual diagnostic criteria: Is it reasonable? Eur Radiol 2007;17:1498–509.

[41] Sinha S, Sinha U. In vivo diffusion tensor imaging of the human prostate. Magn Reson Med 2004;52:530–7.

[42] Pickles MD, Gibbs P, Sreenivas M, et al. Diffusion-weighted imaging of normal and malignant prostate tissue at 3.0 T. J Magn Reson 2006;23:130–4.

[43] Gibbs P, Liney GP, Pickles MD, et al. Correlation of ADC and T2 measurements with cell density in prostate cancer at 3.0 Tesla. Investig Radiol 2009;44:572–6.

[44] Haider MA, van der Kwast TH, Tanguay J, et al. Combined T2-weighted and diffusion-weighted MRI for localization of prostate cancer. Am J Roentgenol 2007;189:323–8.

[45] van As N, Charles-Edwards E, Jackson A, et al. Correlation of diffusion-weighted MRI with whole mount radical prostatectomy specimens. Br J Radiol 2008;81:456–62.

[46] Yoshimitsu K, Kiyoshima K, Irie H, et al. Usefulness of apparent diffusion coefficient map in diagnosing prostate carcinoma: Correlation with stepwise histopathology. J Magn Reson 2008;27:132–9.

[47] Mazaheri Y, Hricak H, Fine SW, et al. Prostate tumor volume measurement with combined T2-weighted imaging and diffusion-weighted MR: Correlation with pathologic tumor volume. Radiology 2009;252:449–57.

[48] Woodfield CA, Tung GA, Grand DJ, et al. Diffusion-weighted MRI of peripheral zone prostate cancer: Comparison of tumor apparent diffusion coefficient with Gleason score and percentage of tumor on core biopsy. Am J Roentgenol 2010;194:W316–22.

[49] de Souza N, Reinsberg S, Scurr E, et al. Magnetic resonance imaging in prostate cancer: The value of apparent diffusion coefficients for identifying malignant nodules. Br J Radiol 2007;80:90–5.

[50] de Souza N, Riches S, Vanas N, et al. Diffusion-weighted magnetic resonance imaging: A potential non-invasive marker of tumor aggressiveness in localized prostate cancer. Clin Radiol 2008;63:774–82.

[51] van As NJ, de Souza NM, Riches SF, et al. A study of diffusion-weighted magnetic resonance imaging in men with untreated localized prostate cancer on active surveillance. Eur Urol 2009;56:981–8.

[52] Lee SH, Park KK, Choi KH, et al. Is endorectal coil necessary for the staging of clinically localized prostate cancer? Comparison of non-endorectal vs. endorectal MR imaging. World J Urol 2010;28:667–72.

[53] Bax J, Cool D, Gardi L, et al. Mechanically assisted 3D ultrasound guided prostate biopsy system. Med Phys 2008;35:5397–410.

[54] Marks L, Ward A, Gardi L, et al. Tracking of prostate biopsy sites using a 3D ultrasound device (Artemis). J Urol 2010;183:e832.

[55] Rankin R, Fenster A, Downey D, et al. Three-dimensional sonographic reconstruction: Techniques and diagnostic applications. Am J Roentgenol 1993;161:695–702.

[56] Ahmed HU, Kirkham A, Arya M, et al. Is it time to consider a role for MRI before prostate biopsy? Nat Rev Clin Oncol 2009;6:197–206.

[57] Raz O, Haider M, Trachtenberg J, et al. MRI for men undergoing active surveillance or with rising PSA and negative biopsies. Nat Rev Urol 2010;7:543–51.

[58] Rosset A, Spadola L, Ratib O. OsiriX: An open-source software for navigating in multidimensional DICOM images. J Digit Imag 2004;17:205–16.

[59] Ladak H, Mao F, Wang Y, et al. Prostate boundary segmentation from 2D ultrasound images. Med Phys 2000;27:1777–88.

[60] Wang Y, Cardinal N, Downey D, et al. Semi-automatic 3D segmentation of the prostate using 2D ultrasound images. Med Phys 2003;30:88–97.

[61] Narayanan R, Kurhanewicz J, Shinohara K, et al. MRI-ultrasound registration for targeted prostate biopsy. IEEE Intl Symp Biomed Imaging 2009;991–4.

[62] Karnik V, Fenster A, Bax J, et al. Assessment of image registration accuracy in 3-dimensional transrectal ultrasound guided prostate biopsy. Med Phys 2010;37:802–13.